

Violent interaction between the AGN and the hot gas in the core of the galaxy cluster Sérsic 159-03

N. Werner¹★, M. Sun², J. Bagchi³, S. W. Allen¹, G. B. Taylor⁴†, S. K. Sirothia⁵, A. Simionescu¹‡, E. T. Million⁶, J. Jacob⁷, M. Donahue⁸

¹Kavli Institute for Particle Astrophysics and Cosmology, Stanford University, 452 Lomita Mall, Stanford, CA 94305-4085, USA and SLAC National Accelerator Laboratory, 2575 Sand Hill Road, Menlo Park, CA 94025, USA

²Department of Astronomy, University of Virginia, P.O. Box 400325, Charlottesville, VA 22904-4325, USA

³Inter University Center for Astronomy and Astrophysics (IUCAA), Post Bag 4, Ganeshkhind, Pune 411 007, India

⁴Department of Physics and Astronomy, University of New Mexico, Albuquerque, NM 87131, USA

⁵National Centre for Radio Astrophysics, Tata Institute of Fundamental Research, Post Bag 3, Ganeshkhind, Pune 411007, India

⁶Department of Physics and Astronomy, University of Alabama, Box 870324, Tuscaloosa, AL 35487, USA

⁷Department of Physics, Newman College, Thodupuzha 685 585, India

⁸Physics&Astronomy Department, Michigan State University, East Lansing, MI 48824-2320, USA

13 January 2013

ABSTRACT

We present a multi-wavelength study of the energetic interaction between the central active galactic nucleus (AGN), the intra-cluster medium, and the optical emission line nebula in the galaxy cluster Sérsic 159-03. We use X-ray data from *Chandra*, high resolution X-ray spectra and UV images from *XMM-Newton*, *H α* images from the *SOAR* telescope, *HST* optical imaging, and *VLA* and *GMRT* radio data. The cluster center displays signs of powerful AGN feedback, which has cleared the central regions ($r < 7.5$ kpc) of dense, X-ray emitting ICM. X-ray spectral maps reveal a high pressure ring surrounding the central AGN at a radius of $r \sim 15$ kpc, indicating an AGN driven weak shock. The cluster harbors a bright, 44 kpc long *H α* +*[N II]* filament extending from the centre of the cD galaxy to the north. Along the filament, we see low entropy, high metallicity, cooling X-ray gas. The gas in the filament has most likely been uplifted by ‘radio mode’ AGN activity and subsequently stripped from the galaxy due to its relative southward motion. Because this X-ray gas has been removed from the direct influence of the AGN jets, part of it cools and forms stars as indicated by the observed dust lanes, molecular and ionized emission line nebulae, and the excess UV emission.

Key words: X-rays: galaxies: clusters – galaxies: individual: Sérsic 159-03 – galaxies: intergalactic medium – cooling flows

1 INTRODUCTION

Supermassive black holes (SMBH) play a crucial role in galaxy formation. The correlation between the mass of the central SMBH and the bulge mass of their host galaxies suggests that their evolution is tightly coupled (Magorrian et al. 1998). Outbursts of accreting SMBH (referred to as active galactic nuclei or AGN) disturb and heat the surrounding gas, lowering the accretion rate and, in some cases, driving so much gas out of the galaxy that the star formation is drastically reduced.

The most dramatic portrayal of the interaction between AGN and their surroundings can be seen in the distribution of X-ray emitting gas in nearby giant ellipticals and clusters of galaxies. *Chan-*

dra X-ray images have revealed giant cavities and shocks in the hot gas produced by repeated outbursts of the central AGN (e.g. Fabian et al. 2003; Nulsen et al. 2005; Forman et al. 2005). These AGN outbursts in principle provide enough power to offset radiative losses, suppress cooling, and prevent further star formation in the dense cores of clusters of galaxies (see e.g. McNamara & Nulsen 2007). Detailed X-ray imaging and 2D spectral mapping of cooling cores with cavities, X-ray bright filaments, and shock fronts, provides the most reliable means of measuring the energy injected into the hot intra-cluster medium (ICM) by AGN, and is a powerful tool to study the physics of the AGN feedback in general (see e. g. Randall et al. 2011; Million et al. 2010b; Werner et al. 2010; Simionescu et al. 2009b).

Here we present a detailed multi-wavelength study of AGN feedback processes in the core of the nearby ($z=0.0564$; Maia et al. 1987), relatively poor, low mass cluster of galaxies Sérsic 159-03 (A S1101). The thermal properties and chemical enrichment of the

★ Chandra/Einstein fellow, E-mail: norbertw@stanford.edu

† Adjunct Astronomer at the National Radio Astronomy Observatory

‡ Einstein fellow

hot ICM in this cooling core cluster have been studied in detail using *XMM-Newton* (Kaastra et al. 2001, 2004; de Plaa et al. 2006). Compared to other cooling core clusters, where the central temperature drops to $\sim 1/3$ of the peak ambient value, Sérsic 159-03 has a relatively modest (factor of 1.5) temperature drop in the core (Sun et al. 2009). The radio properties of this cluster have been reported by Bîrzan et al. (2008), in the study of a sample of 24 cooling cores. The bright optical emission line nebulae in the core of the cluster have been studied in detail by Crawford & Fabian (1992) and more recently by Oonk et al. (2010) using integral field spectroscopy.

Throughout the paper we adopt a flat Λ_{CDM} cosmology with $H_0 = 70 \text{ km s}^{-1} \text{ Mpc}^{-1}$ and $\Omega_M = 0.3$, which implies a linear scale of $1.2 \text{ kpc arcsec}^{-1}$ at the cluster redshift of $z = 0.0564$ (Maia et al. 1987). Throughout the paper, abundances are given with respect to the solar values by Grevesse & Sauval (1998). All errors are quoted at the 68 per cent confidence level.

2 DATA REDUCTION AND ANALYSIS

2.1 Optical, $H\alpha$, and UV data

To study the optical properties of the central cluster galaxy, we analyzed a 600 s observation available in the *HST* archive (proposal ID: 8719). The image was taken with WFPC2 using the F555W filter and placing the galaxy onto the WF3 chip.

Narrow-band optical imaging was performed with the 4.1 m *SOAR* telescope on September 13, 2009 (UT) using the *SOAR* Optical Imager (SOI). The night was photometric with a seeing of around $1''$. We used the 6916/78 CTIO narrow-band filter for the $H\alpha + [\text{N II}]$ lines, and the 6738/50 filter for the continuum. We took four 1200 s exposures with the 6916/78 filter and four 750 s exposures with the 6738/50 filter. We reduced each image using the standard procedures in the IRAF MSCRED package using EG 274 as a spectroscopic standard. The pixels were binned 2×2 , for a scale of $0.154''$ per pixel. More details on the SOI data reduction can be found in Sun et al. (2007).

We also analyzed near Ultra Violet data obtained by the *XMM-Newton* Optical Monitor on 2002 November 20–21. Exposures were taken with the UVW1 (2400–3600 Å) and UVW2 (1800–2400 Å) filters.

2.2 Radio data

The summary of radio observations with *GMRT*¹ and *VLA*, including the observation date, obtained beam, and rms noise, is shown in Table 1. The strong, stable calibrator 3C 48 was used for absolute flux density and bandpass calibration at all frequencies. We tied the final flux density scale to the standard ‘Baars-scale’ (Baars et al. 1977). The *VLA* data were obtained in the B configuration. Their calibration was performed using AIPS (Greisen 2003) in the standard fashion, while imaging and self-calibration were performed using *Di fmap* (Shepherd et al. 1995).

The *GMRT* data were reduced using AIPS++ (version: 1.9). After applying bandpass corrections to the phase calibrator, gain and phase variations were estimated, and flux density, bandpass, gain and phase calibration were applied. The data for antennas with high errors in antenna-based solutions were examined and flagged over certain time ranges. Some baselines were also flagged based

on closure errors on the bandpass calibrator. Channel and time-based flagging of data points corrupted by radio frequency interference (RFI) was applied using a median filter with a 6σ threshold. Residual errors above 5σ were also flagged after a few rounds of imaging and self calibration. The system temperature (T_{sys}) was found to vary with antenna, the ambient temperature and elevation (Sirothia 2009). In the absence of regular T_{sys} measurements for *GMRT* antennas, this correction was estimated from the residuals of corrected data with respect to the model. The corrections were then applied to the data. The final images were made after several rounds of phase self calibration, and one round of amplitude self calibration, where the data were normalized by the median gain for all the data.

2.3 Chandra X-ray data

The *Chandra* observations of Sérsic 159-03 were taken in August 2009 using the Advanced CCD Imaging Spectrometer (ACIS). The total net exposure time after cleaning is 89.6 ks. We follow the data reduction procedure described in Million et al. (2010a) and Million et al. (2010b). Background spectra were extracted from the appropriate recent blank-sky fields available from the Chandra X-ray Center. These were normalized by the ratio of the observed and blank-sky count rates in the 9.5–12 keV band.

Background subtracted images were created in 13 narrow energy bands, spanning 0.5–7.5 keV. These were flat fielded with respect to the median energy for each image. The blank sky background fields were processed in an identical way to the source observation and reprojected to the same coordinate system. The background subtracted and exposure corrected images were co-added to create the broad band images.

For the spectral analysis, point sources were excluded. The individual regions for the 2D spectral mapping were determined using the Contour Binning algorithm (Sanders 2006), which groups neighboring pixels of similar surface brightness until a desired signal-to-noise threshold is met. In order to have small enough regions to resolve substructure and still have enough counts to achieve better than 7 per cent accuracy in the temperature determination, we adopted a signal-to-noise ratio of 35 (~ 1230 counts per region). Separate photon-weighted response matrices and effective area files were constructed for each region analyzed.

Spectral modeling has been performed with the SPEX package (SPEX uses an updated version of the MEKAL plasma model with respect to XSPEC, Kaastra et al. 1996) in the 0.6–7.0 keV band. To each bin we fitted a model consisting of absorbed (Galactic $N_{\text{H}} = 1.14 \times 10^{20} \text{ cm}^{-2}$, Kalberla et al. 2005) collisionally ionized equilibrium plasmas with temperature, spectral normalization (emission measure), and metallicity as free parameters.

2.4 XMM-Newton RGS data

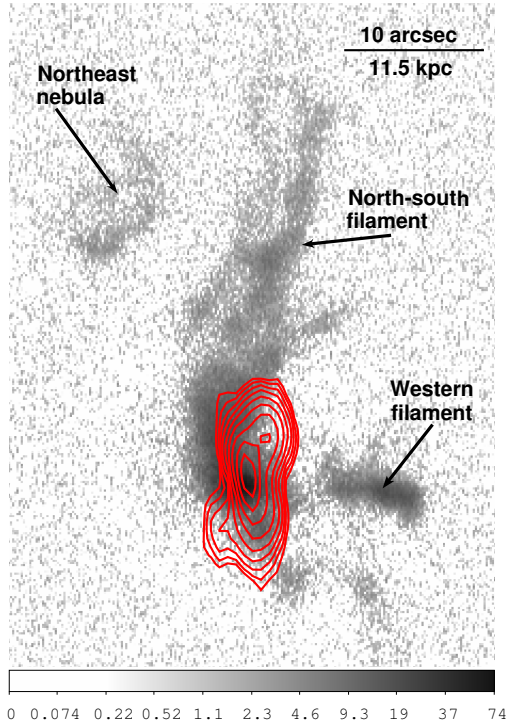
The hot plasma in the core of Sérsic 159-03 exhibits a complex multi-temperature structure (de Plaa et al. 2006). In order to determine the amount of low-temperature cooling X-ray gas in the core and obtain upper limits on the mass deposition rate, we analyze high spectral resolution *XMM-Newton* Reflection Grating Spectrometer (RGS) X-ray data.

The *XMM-Newton* RGS data were obtained on November 20–21 2002, with a net exposure time of 86.3 ks. The data were processed as described in de Plaa et al. (2006). Spectra were extracted from a $4'$ wide extraction region, centred on the optical centre of

¹ The *GMRT* is a national facility operated by the National Centre for Radio Astrophysics of the TIFR, India.

Table 1. Summary of the radio observations. Columns list the central frequency, the telescope array, the resolution of the beam, its position angle, the rms noise, and the observing date.

Frequency (MHz)	Array	Resolution (arcsec)	P.A. (deg)	rms Noise ($\mu\text{Jy beam}^{-1}$)	Obs. date
244	GMRT	20.04×8.92	11.0	1420	2007 November 2, 3
325	GMRT	17.67×9.08	-179.4	352	2009 May 16,17
617	GMRT	8.29×3.13	9.7	250	2009 May 09,11
1400	VLA-B	10×4	0.0	64	2006 August 8
8400	VLA-B	3.1×0.72	8.3	21	2006 August 8

**Figure 1.** $\text{H}\alpha + [\text{N II}]$ image obtained with the 4.1 m SOAR telescope. The image shows a large 44 kpc long north-south filament, a smaller western filament, and a separate nebula at the northeast. The northern end of the large filament separates into two parallel structures. The contours of the 8.4 GHz radio emission are over-plotted in red.

the galaxy. Because the RGS operates without a slit, it collects all photons from within the $4' \times \sim 12'$ field of view. Line photons originating at angle $\Delta\theta$ (in arcminutes) along the dispersion direction are shifted in wavelength by $\Delta\lambda = 0.138\Delta\theta \text{ \AA}$. Therefore, every line is broadened by the spatial extent of the source. To account for this spatial broadening in our spectral model, we produce a predicted line spread function (LSF) by convolving the RGS response with the surface brightness profile of the cluster derived from the EPIC/MOS1 image along the dispersion direction. Because the radial profile of a particular spectral line can be different from the overall radial surface brightness profile, the line profile is multiplied by a scale factor s , which is the ratio of the observed LSF to the expected LSF. This scale factor is a free parameter in the spectral fit. We fit the spectra in the 8–28 \AA band.

3 RESULTS

3.1 Optical and UV properties

The cooling core of Sérsic 159-03 harbors a remarkable $\text{H}\alpha + [\text{N II}]$ emission line filament system shown in Fig. 1. This system of emission line nebulae consists of a large 44 kpc long north-south filament extending to the radius of 35 kpc in the north and a smaller western structure extending out to 16 kpc. The total $\text{H}\alpha + [\text{N II}]$ flux is $5.9 \times 10^{-14} \text{ erg s}^{-1} \text{ cm}^{-2}$. Assuming $[\text{N II}]_{6583\text{\AA}}/\text{H}\alpha = 1$ and $[\text{N II}]_{6548\text{\AA}}/[\text{N II}]_{6583\text{\AA}} = 0.35$, the total $\text{H}\alpha$ flux is $\sim 2.5 \times 10^{-14} \text{ erg s}^{-1} \text{ cm}^{-2}$. The total luminosity of the $\text{H}\alpha$ line emission (with the $[\text{N II}]$ flux excluded) is $L_{\text{H}\alpha} = 2 \times 10^{41} \text{ ergs s}^{-1}$. Our measured $\text{H}\alpha$ flux is higher than the flux $f_{\text{H}\alpha} = 1.79 \pm 0.15 \times 10^{-14} \text{ erg s}^{-1} \text{ cm}^{-2}$ measured by McDonald et al. (2010), who used a filter with a 10 times narrower bandpass targeting only the $\text{H}\alpha$ emission lines. A separate nebula can be seen 25 kpc to the northeast of the core.

Assuming a volume filling fraction of unity, a cylindrical geometry in the $\text{H}\alpha$ bright regions, optically thin ionized gas, isotropic radiation, and case B recombination at 10^4 K (Bland-Hawthorn & Maloney 1999), the total mass of the $\text{H}\alpha$ emitting gas is about $2.7 \times 10^9 M_{\odot}$. However, these optical filaments most likely consist of many thin threads with very small volume filling fractions (e.g. Fabian et al. 2008). The inferred mass is therefore likely to be significantly overestimated.

The giant elliptical galaxy in the core of Sérsic 159-03 has its major axis aligned in the northeast-southwest direction (left panel of Fig. 2). The HST data reveal a 4.5 kpc long dust lane extending from the centre to the north, coincident with the bright $\text{H}\alpha$ emitting gas. It is displaced to the east from the core of the galaxy by about $1.2''$ ($\sim 1.4 \text{ kpc}$). The dust lane is clearly visible in the middle panel of Fig. 2, where the HST image is divided by the best fit 2D elliptical de Vaucouleurs model. This ratio image also uncovers a fainter dust lane to the south of the core. The over-subtraction of the emission from center of the galaxy by the model shows that the surface brightness of the stellar core is flatter than the de Vaucouleurs profile. We do not detect optical emission from the AGN.

Near Ultra Violet images (NUV) from the *XMM-Newton* Optical Monitor show diffuse emission which is co-spatial with the dust lanes and the emission line nebulae, providing a strong indication for current star-formation (right panel of Fig. 2). After correcting for coincidence, dead-time loss, and time sensitivity degradation, the total UVW1 luminosity within a radius of 7 arcsec is $3.7 \times 10^{42} \text{ ergs s}^{-1}$. Based on Cardelli et al. (1989), the Galactic extinction in the UVW1 band was assumed to be 0.07 mag and the unknown internal extinction was set to zero. We measured the 2MASS J-band luminosity within the same aperture and subtracted the contribution from the passive stellar population from the empirical $L_{\text{UVW1}} - L_{\text{J}}$ relation derived by Hicks & Mushotzky (2005). We find a net NUV

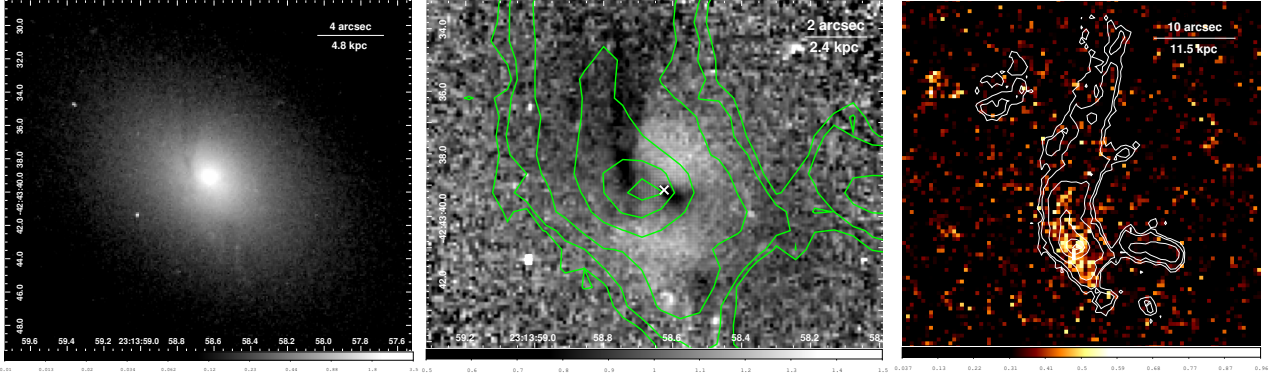


Figure 2. *Left panel:* *HST* image of the central cluster galaxy of Sérsic 159-03 with clear dark dust bands. *Middle panel:* The *HST* image divided by the best fit 2D elliptical de Vaucouleurs model of the galaxy. The white “X” mark indicates the optical center of the galaxy. A 4.5 kpc long dust lane displaced to the east and extending to the north is clearly visible. The inner region of the galaxy is disturbed and not well described by the de Vaucouleurs profile. The green contours show the isophotes of the $H\alpha$ + $[N II]$ filaments (see Fig. 1). *Right panel:* *XMM-Newton* Optical Monitor UVW2 (1800–2400 Å) image of the core of the galaxy with the $H\alpha$ contours over-plotted. The UV emission clearly extends along the brightest region of the $H\alpha$ filament.

Table 2. Radio flux densities. The flux densities obtained by GMRT and VLA are from this work, the values obtained at 408 MHz and 843 MHz by MOST are from the MRC (Large et al. 1981) and SUMSS surveys (Bock et al. 1999; Mauch et al. 2003). The flux density at 4.75 GHz obtained by ATCA is from Hogan et al. in preparation.

Frequency (MHz)	Array	Flux density (Jy)
244	GMRT	3.360 ± 0.20
325	GMRT	2.024 ± 0.20
408	MOST	1.390 ± 0.10
617	GMRT	0.786 ± 0.05
843	MOST	0.472 ± 0.014
1425	VLA-B	0.235 ± 0.020
4752	ATCA	0.0469 ± 0.007
8400	VLA-B	0.0313 ± 0.005

luminosity excess of $\sim 2.3 \times 10^{42}$ ergs s^{-1} . Without correcting for internal extinction, we obtain a UVW2–UVW1 color ~ 0.4 mag.

3.2 Radio morphology

The contours of the 8.4 GHz radio emission in Fig. 1 and 3 resolve the source into an S-shape, oriented primarily north-south, with a compact central feature of flux density 6.3 mJy/beam, which is approximately the fifth of the total radio flux at this frequency. The jets seem to start out in the northeast-southwest direction, before bending clockwise. At 1.4 GHz the total flux density is ~ 230 mJy and shows a core with an extension ~ 12 arcseconds to the east (see the white contours in Fig. 4). The centers of the radio and optical emission are well aligned. At the 617 MHz *GMRT* radio map, the morphology of the radio emission is nearly identical to 1.4 GHz. The extension to the east is robustly detected at 617 MHz and seems to be divided into two filaments. The lower frequency GMRT radio maps do not significantly resolve the radio source.

In the left panel of Fig. 3 we show a red+green color image, produced from the radio data at 617 MHz (red) and 1.4 GHz (green) with the contours of the 8.4 GHz radio emission overplotted. This combined radio image clearly shows the extension to the east. The

central panel of Fig. 3 shows the spectral index map of the core of Sérsic 159-03 produced by combining the 617 MHz *GMRT* and the 1.4 GHz *VLA* radio data. Only data above 2 mJy/beam at 617 MHz and 0.2 mJy/beam at 1.4 GHz were included. To the east, north-east and north-west of the core the radio emission has a very steep spectrum described by a power-law $S_\nu \propto \nu^{-\alpha}$ with index $\alpha > 2.2$. The spectrum of the central region is flatter with index $\alpha \sim 1$.

In Table 2 we show the integrated radio flux densities at five different frequencies obtained with *GMRT* and *VLA*. We also list the published flux densities obtained by the MRC survey at 408 MHz (Large et al. 1981) and by the SUMSS survey at 843 MHz (Bock et al. 1999; Mauch et al. 2003) performed with the Molonglo Observatory Synthesis Telescope (MOST). The integrated flux density at 4.75 GHz obtained by the Australia Telescope Compact Array (ATCA) is from Hogan et al. in preparation. The broad band radio spectrum is shown in the right panel of Fig. 3. Between 244 MHz and 1.4 GHz the integrated spectrum can be described by a power-law $S_\nu \propto \nu^{-\alpha}$ with $\alpha = 1.49$. At high frequencies, between 4.8 GHz and 8.4 GHz, however, the best fit power-law is significantly flatter with index $\alpha = 0.71$.

3.3 X-ray imaging: a disturbed morphology

The X-ray data show no evidence for a point source associated with the central radio source. Assuming a power-law like spectrum with a photon index $\Gamma = 2.0$, a conservative upper limit on the X-ray flux in the 2–10 keV band is $f_X = 2.3 \times 10^{-15}$ erg s^{-1} cm^{-2} . The large scale X-ray emission from the cluster is elongated in the same northeast-southwest direction as the major axis of the cD galaxy. The X-ray emission does not show obvious sharp surface brightness discontinuities, indicative of cold fronts due to sloshing gas.

While the large scale X-ray morphology of Sérsic 159-03 is relatively relaxed, its core is strongly disturbed. The brightest, densest X-ray emitting gas is displaced northward from the centre of the cD galaxy to a radius of $r \sim 8$ kpc. In the top left panel of Fig. 4, we show the smoothed *Chandra* image of the cluster core in the 0.5–7.5 keV band. The black cross indicates the position of the central AGN. In the top right panel, we show the same image, with the contours of the $H\alpha$ + $[N II]$ emission over-plotted in black, and the contours of the 8.4 GHz and 1.4 GHz radio emission over-plotted in blue and white, respectively. The lower panels of Fig. 4

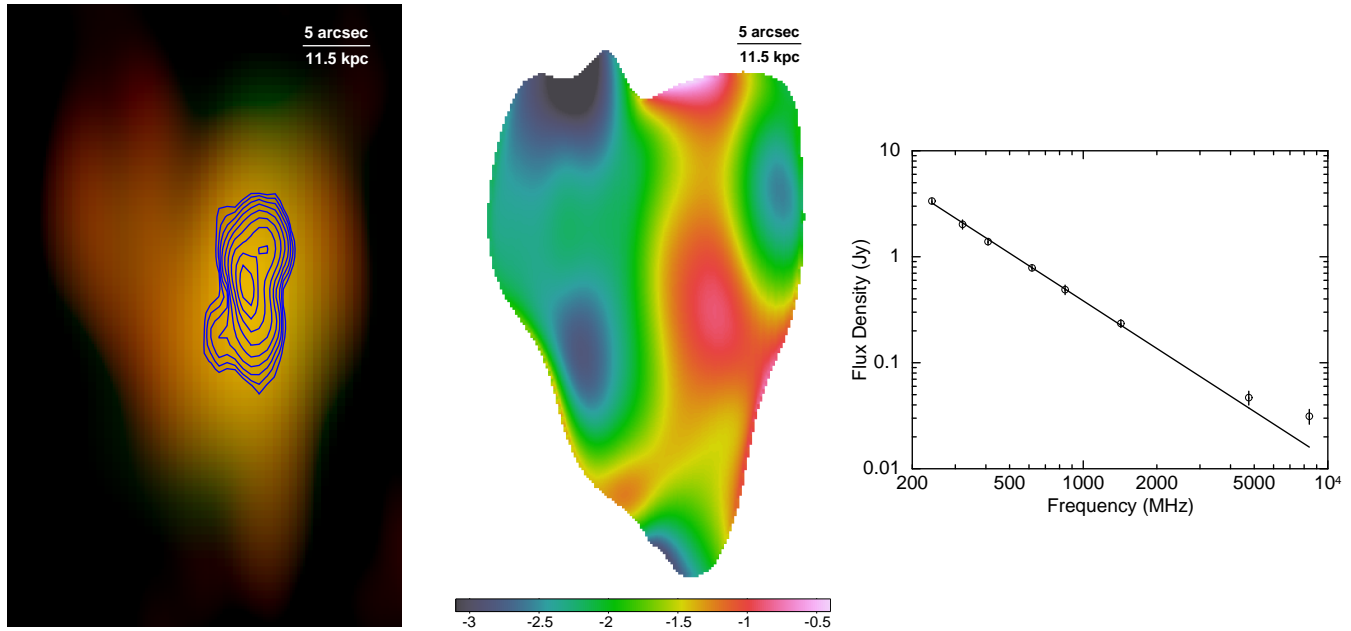


Figure 3. *Left panel:* Red+green color image, produced from the radio data at 617 MHz (red) and 1.4 GHz (green), with the 8.4 GHz radio contours overplotted. *Central panel:* Spectral index map produced by combining the 617 MHz *GMRT* and the 1.4 GHz *VLA* radio data. The radio maps show the innermost 0.5×0.78 arcmin² region of the cluster. The radio maps at the two frequencies have been matched in resolution. *Right panel:* The broad band radio spectrum between 244 MHz and 8.4 GHz. The radio spectrum between 244 MHz and 1.4 GHz can be described by the overplotted power-law $S_\nu \propto \nu^{-\alpha}$ with index $\alpha = 1.49$.

show the same *Chandra* images divided by their best fit 2D elliptical double beta model. The images show a bright ridge of dense thermal X-ray gas displaced by about 8 kpc to the north of the AGN and a clumpy X-ray filament extending along the $H\alpha$ filament to 31 kpc beyond this ridge. Another X-ray filament extends to the west and coincides with the western optical emission line nebula.

The ridge of dense, thermal X-ray emitting gas to the north of the AGN seems to be interacting with, and confining, the 8.4 GHz radio emitting plasma (blue contours in Fig. 4). The jets appear distorted by the interaction with the dense cooling gas. The 1.4 GHz radio plasma also appears deflected by the ridge of dense gas to the east, where it fills a gap - an elongated cavity - in the X-ray surface brightness distribution. This elongated cavity is possibly composed of two cavities. The X-ray surface brightness drops sharply to the southeast of the AGN, forming an apparent cavity with a radius of ~ 11 kpc, filled by 1.4 GHz radio emission. This drop in surface brightness is spatially coincident with the sharp southeastern edge of the bright emission line nebulae. A possible ghost cavity with a radius of ~ 10 kpc, with no associated radio emission, can be seen about 30 kpc to the east of the nucleus.

3.4 Thermodynamic properties of the core

The disturbed morphology of the cluster core is also reflected in the 2D maps of density, temperature, entropy, and pressure shown in Fig. 5. The ICM spatially associated with the large north-south $H\alpha$ filament has a relatively low projected temperature (top right panel of Fig. 5). The high density (top left panel of Fig. 5) and low temperature of this feature translate into low entropy (lower left panel of Fig. 5). The western filament, on the other hand, has a significantly higher temperature and entropy.

The projected thermal pressure peaks in an approximate ring

surrounding the core (lower right panel of Fig. 5). The pressure in this ring is approximately 20 per cent higher than in the center. The maps reveal that the relatively over-pressured gas to the southeast of the core has a higher temperature than the surrounding gas, which strongly indicates that it has been compressed and heated by an AGN driven shock.

The metallicity of the ICM along the $H\alpha + [N II]$ filaments is higher than that of the surrounding plasma (see Fig. 6). The apparent metallicities of the bright northern ridge of cooling plasma and of the core are, however, low. It has been shown that the metallicity is sensitive to the modeling of the underlying temperature structure and, if multi-temperature plasma is modeled with a single-temperature spectral model, the metallicity of gas can be significantly underestimated (e.g. Buote 2000). The low metallicities of these features thus indicate the presence of multi-phase gas.

3.5 High resolution X-ray spectra

In order to determine whether cooling X-ray gas with $kT < 1$ keV is present in the core of the cluster, we examine the *XMM-Newton* RGS spectra (see Fig. 7) to search for low temperature line emission (primarily Fe XVII) tracing rapidly cooling gas. We fit the RGS data with a model consisting of collisionally ionized equilibrium plasmas at four fixed temperatures (0.25 keV, 0.75 keV, 1.5 keV, and 3 keV) with variable normalizations and common metal abundances. The abundances of O, Ne, Mg, and Fe are free parameters in the fit. Our fit confirms the presence of relatively cool, $kT < 1$ keV plasma. Based on the lack of O VII line emission however, which is emitted at $kT < 0.4$ keV, we place a strong upper limit on the amount of gas cooling radiatively to very low temperatures. Our 90% confidence upper limit on the emission measure of

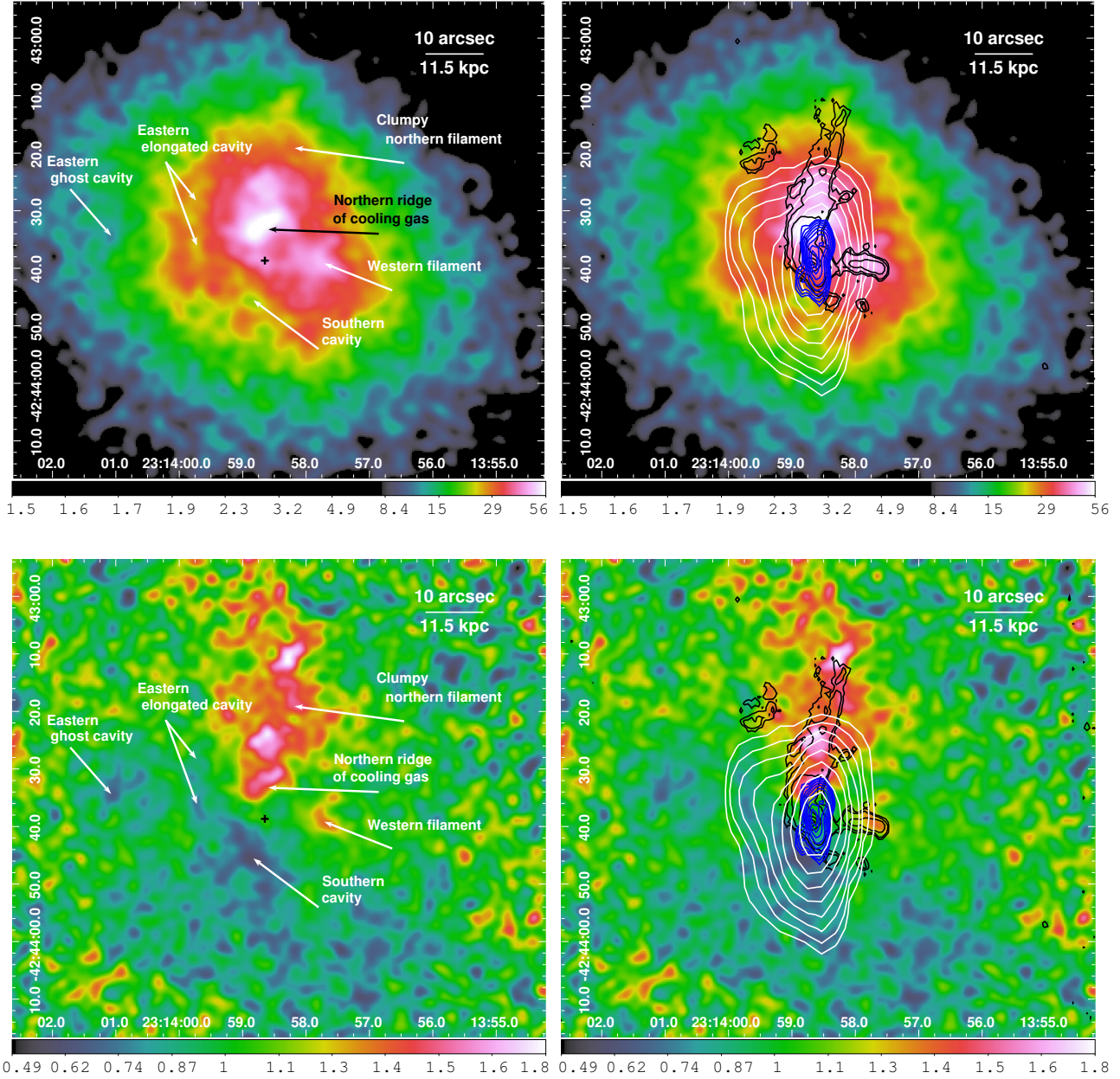


Figure 4. *Top left panel:* Background subtracted, flat-fielded *Chandra* X-ray image of the core of Sérsic 159-03 in the 0.5–7.5 keV band. The cross indicates the position of the central radio source. *Top right panel:* The same *Chandra* image with over-plotted contours of the 8.4 GHz (blue) and 1.4 GHz (white) radio emission, and with the contours of the $H\alpha+[N II]$ line emission (black). The dense cooling gas is displaced to the north of the centre of the galaxy and the region within $r \lesssim 7.5$ kpc is void of dense gas. *Lower left panel:* The *Chandra* image divided by the best fit 2D elliptical double beta model. Note the clear structure to the north. *Lower right panel:* The same ratio image with the contours of the radio and $H\alpha+[N II]$ emission over-plotted. The images have been smoothed with a Gaussian kernel.

gas with $kT = 0.25$ keV is $Y = \int n_{Hn_e} dV = 9 \times 10^{64} \text{ cm}^{-3}$, which is about 50% of the best fit emission measure for the 0.75 keV gas.

In order to place constraints on the amount of cooling in the cluster core we fit the RGS spectra with a separate model consisting of thermal plasma in collisional ionization equilibrium and two isobaric cooling flow models. The first cooling flow model is used to account for gas with temperatures between $kT_{\text{upper}} = 1.9$ keV and $kT_{\text{lower}} = 0.5$ keV, which appears to be the ‘temperature floor’ in several cooling core clusters (Sanders et al. 2009, 2010; Werner et al. 2010). The second cooling flow model is used to place an upper limit on the radiative cooling rate from 0.5 keV

down to cold gas. While in the temperature range of 1.9–0.5 keV the data are formally consistent with a radiative cooling rate of $\dot{M} = 82 \pm 11 M_{\odot} \text{ yr}^{-1}$, the 95% confidence upper limit for radiative cooling from 0.5 keV to lower temperatures is only $25 M_{\odot} \text{ yr}^{-1}$.

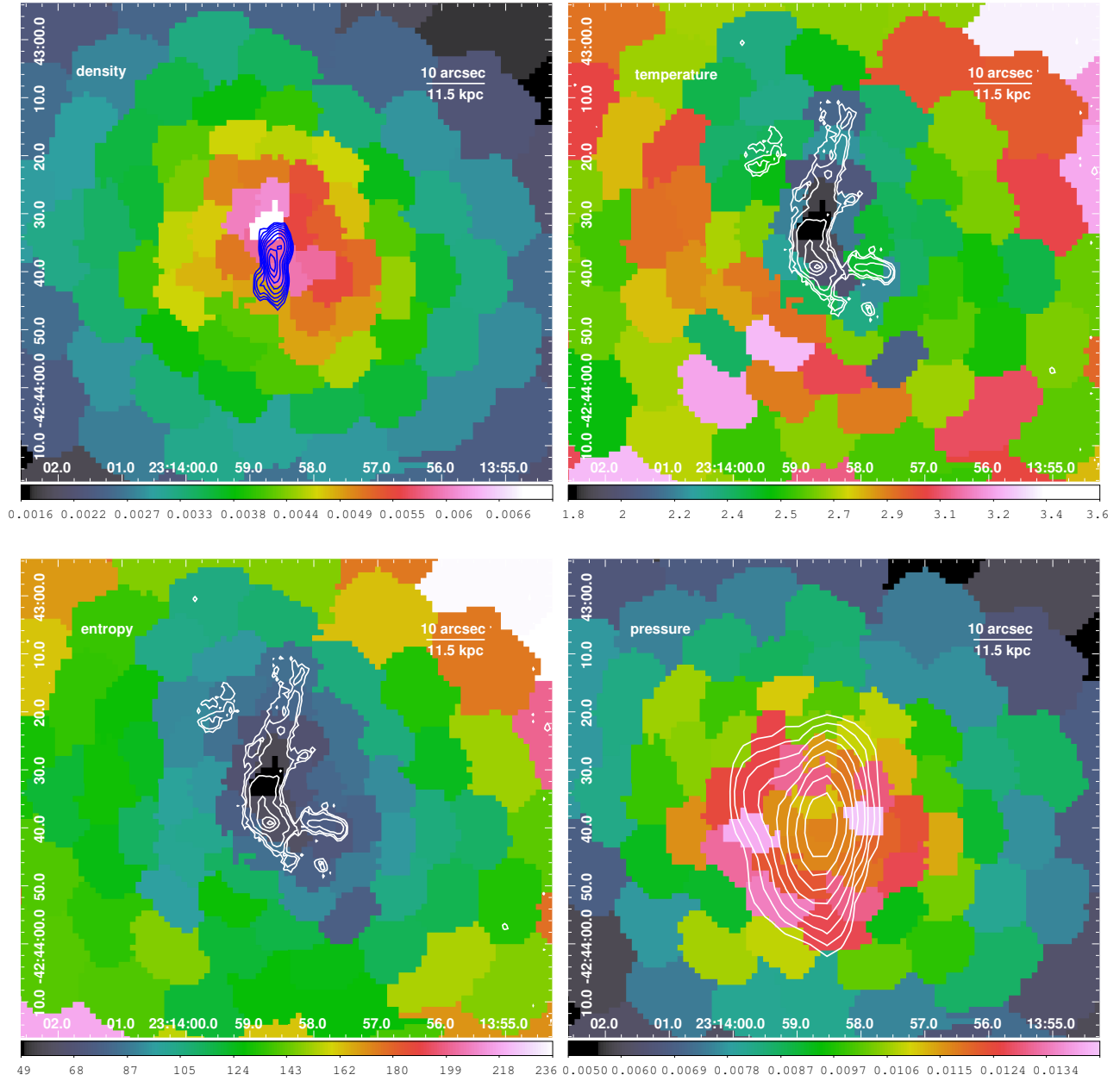


Figure 5. 2D maps of density (in units of cm^{-3} ; top left panel), temperature (in units of keV; top right panel), pressure (in units of $\text{keV cm}^{-3} \times \left(\frac{l}{2\text{Mpc}}\right)^{-1/2}$; lower right panel), and entropy (in units of $\text{keV cm}^2 \times \left(\frac{l}{2\text{Mpc}}\right)^{1/3}$; lower left panel). The maps were obtained by fitting each S/N \sim 35 region independently with a single temperature thermal model, yielding 1σ fractional uncertainties of ~ 10 per cent on the temperature. The contours of the $\text{H}\alpha$ + $[\text{N II}]$ optical line emission are over-plotted on the temperature and entropy maps. The contours of the 8.4 GHz and 1.4 GHz radio emission are over-plotted on the density and pressure map, respectively.

4 DISCUSSION

4.1 Displacement of gas from the cD galaxy

The core of Sérsic 159-03 has a remarkably complex and rich morphology at all wavelengths. It displays signs of a powerful AGN feedback. The central regions of the galaxy ($r < 7.5$ kpc) are cleared of the densest, X-ray emitting ICM and the cluster core displays a massive, bright $\text{H}\alpha$ filament extending northward from the centre of the cD galaxy to a radius of 35 kpc. This long filament

is reminiscent of that in Abell 1795 (Fabian et al. 2001; Crawford et al. 2005; McDonald & Veilleux 2009).

While the densest cooling X-ray plasma has been pushed away and uplifted from the cooling core by the radio jets to a radius of at least $r \sim 8$ kpc, the brightest core of the $\text{H}\alpha$ emission is not displaced from the galactic nucleus. The most likely reason is that the $\text{H}\alpha$ emitting gas is only a thin layer on an underlying large reservoir of dense atomic and molecular gas at the base of the galaxy potential, which is difficult to uplift entirely. Observations of K-band emission lines of molecular and ionized hydrogen with the

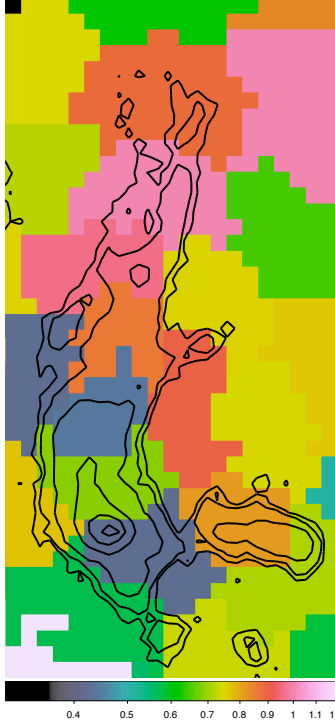


Figure 6. Metallicity map of the core of the cluster with the contours of the $H\alpha + [N II]$ optical line emission over-plotted. The metallicity of the ICM along the filament is higher than that of the surrounding medium. The apparent metallicity of the bright ‘northern ridge’ and of the core is low, indicating the presence of multi-phase gas.

SINFONI integral field spectrograph reveal extended filaments in the core of Sérsic 159-03, tracing closely each other and the $H\alpha$ emission (Oonk et al. 2010). The line-of-sight velocities, as measured by Oonk et al. (2010), show a striking east/west dichotomy, suggesting that part of the velocity vector of the jets, which push and uplift the gas, is oriented along our line of sight. The gas to the east of the stellar core has a radial velocity of $\sim 200 \text{ km s}^{-1}$ with respect to the cD galaxy, which seems to be decreasing with the distance from the nucleus.

The radial velocity distribution of the gas along the western filament goes smoothly from about -200 km s^{-1} to 50 km s^{-1} with increasing distance from the core. These velocity gradients indicate that the gas has been pushed out by the jets of the AGN.

The morphology of the cooling filamentary gas indicates relative gas motions with the ambient ICM moving toward the northwest, dragging and bending the $H\alpha$ filament. The gas uplifted by the jet in the southwestern direction has been dragged to the west and the gas uplifted towards northeast has been displaced in the north-northwestern direction. These relative gas motions are most likely the result of the south-southeastward peculiar motion of the cD galaxy.

Relatively cool X-ray gas is present along the whole northern filament of Sérsic 159-03, but the correlation between the $H\alpha$ and soft X-ray emission is not perfect. We see clumps of dense, cooling X-ray emitting plasma at $\sim 8 \text{ kpc}$ and at $\sim 17 \text{ kpc}$, but no obvious $H\alpha$ peaks at the same locations. The ‘northern ridge’ at $r \sim 8 \text{ kpc}$ has the coldest projected temperature and lowest entropy. The X-ray filament extends to the north by about 3 kpc further than the observed $H\alpha$ filament. The western $H\alpha + [N II]$ filament is also sur-

Table 3. Best fit parameters for a four-temperature fit and a CIE+two-cooling-flow model fit to the high-resolution RGS spectra extracted from a $4'$ wide region centred on the core of Sérsic 159-03. Emission measures, $Y = \int n_H n_e dV$, are given in 10^{66} cm^{-3} . Radiative cooling rates are given in $M_\odot \text{ yr}^{-1}$. The scale factor s is the ratio of the observed LSF to the expected LSF based on the overall radial surface brightness profile. The upper limits are quoted at their 95 per cent confidence level. Abundances are quoted with respect to the values of Grevesse & Sauval (1998).

Parameter	4T-model	CIE+c.f.+c.f. model
$Y_{0.25\text{keV}}$	0.05 ± 0.04	—
$Y_{0.75\text{keV}}$	0.19 ± 0.03	—
$Y_{1.5\text{keV}}$	0.7 ± 0.3	—
$Y_{3.0\text{keV}}$	12.1 ± 0.3	—
Y_{CIE}	—	12.3 ± 0.2
$\dot{M}_{1.9-0.5\text{keV}}$	—	82 ± 11
$\dot{M}_{0.5-0.1\text{keV}}$	—	< 25
kT (keV)	—	3.05 ± 0.16
s	1.12 ± 0.13	1.13 ± 0.11
O	0.39 ± 0.04	0.43 ± 0.04
Ne	0.43 ± 0.12	0.44 ± 0.11
Fe	0.78 ± 0.04	0.82 ± 0.06

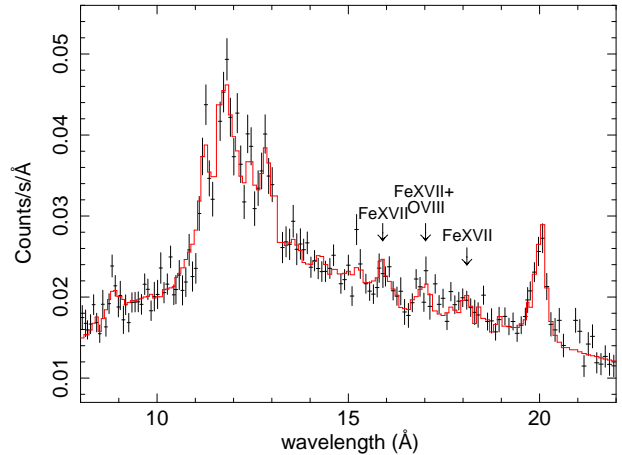


Figure 7. The first order *XMM-Newton* RGS spectrum extracted from a $4'$ wide region centred on the core of Sérsic 159-03. The continuous line represents the best fit model to the spectrum. Fe XVII lines emitted by plasma with $kT < 0.9 \text{ keV}$ are clearly visible in the spectrum.

rounded by bright, dense X-ray emitting gas, but its projected temperature is $\sim 0.8 \text{ keV}$ higher. The relatively high metallicity of the filament compared to the ambient plasma (see Fig. 6) indicates that the filamentary system has been uplifted and stripped from the cD galaxy.

Gas uplift by buoyant radio-emitting plasma, supplied by the jets of the AGN, has also been observed in other cooling core clusters. Detailed spectroscopic mapping of the cooling core of the Virgo Cluster, centered on M87, shows clearly that radio mode AGN feedback is highly efficient in stripping the core of the galaxy of its lowest entropy gas (Werner et al. 2010). The total mass of uplifted gas in M87 is $6-9 \times 10^8 M_\odot$, which is similar to the current gas mass within its innermost $r \sim 3.8 \text{ kpc}$ region. The disruption of the

core of Sérsic 159-03 is considerably larger than that of M87, but by no means extreme. The AGN feedback in the Hydra A cluster is responsible for the uplift of a few times $10^9 M_\odot$ of low entropy plasma (Simionescu et al. 2009a). Recently, Ehlert et al. (2010) presented a multi-wavelength study of the cluster MACS J1931.8-2634 where extreme AGN feedback with a jet power of $P_{\text{jet}} \sim 10^{46} \text{ erg s}^{-1}$ and the sloshing gas disrupted the core, separating it into two X-ray bright ridges, which are currently at a distance of $\sim 25 \text{ kpc}$ from the core.

4.2 Cooling of the displaced gas and star-formation

To the north of the AGN, we see cooling X-ray plasma displaced by about 8 kpc from the nucleus, producing a prominent bright ridge which confines the high frequency radio plasma. The northern X-ray filament extends 31 kpc beyond this ridge. The relatively dense uplifted X-ray emitting gas, which is removed from the direct influence of the AGN jets, will cool in the absence of heating and eventually form stars. Multiphase cooling X-ray gas, displaced from the center of the cD galaxy and spatially coincident with $\text{H}\alpha$ emission, has also been seen in the Ophiuchus Cluster, in Abell 2052, and in MACS J1931.8-2634 (Million et al. 2010b; Edwards et al. 2009; de Plaa et al. 2010; Ehlert et al. 2010).

Assuming that the filament has been uplifted at half of the sound speed (at 400 km s^{-1}), the age of the filament will be $\sim 10^8 \text{ yr}$. That is approximately equal to the cooling time of 1 keV plasma in pressure equilibrium with the ambient ICM at the observed location. The *XMM-Newton* RGS spectra clearly reveal Fe xvii line emission associated with gas cooling to $kT < 1 \text{ keV}$. The 95 per cent confidence upper limit on radiative cooling below 0.5 keV is $25 M_\odot \text{ yr}^{-1}$.

The densest and coolest X-ray emitting clumps, in particular the bright multiphase ‘northern ridge’, will cool and form narrow $\text{H}\alpha$ emitting filaments (e.g. see simulations by Sharma et al. 2010). It is possible that a significant fraction of the $\text{H}\alpha$ emitting gas in the northern filament at large radii is due to the cooling of the uplifted X-ray emitting plasma. The cold gas is likely to go on to eventually form stars. The *XMM-Newton* OM UVW2 and *Galex* images (McDonald et al. 2010) indicate that the UV emission is extended along the brightest regions of the northern $\text{H}\alpha$ filament, indicating ongoing star formation.

The HST images show that the brightest regions of the filament are dusty. An infrared survey with the *Spitzer Space Telescope*, however, did not detect the system at $70\mu\text{m}$ (Quillen et al. 2008) indicating that the filaments do not contain an exceptionally large amount of warm dust. The excess UV emission from the cD galaxy corresponds to a star-formation rate of $\sim 2.3 M_\odot \text{ yr}^{-1}$ for the assumed Salpeter IMF. Assuming the Kennicutt (1998) relation, $\text{SFR} (M_\odot \text{ yr}^{-1}) = 7.9 \times 10^{-42} (L_{\text{H}\alpha}/\text{erg s}^{-1})$, and neglecting intrinsic extinction due to dust, the measured $\text{H}\alpha$ luminosity corresponds to a star-formation rate of $1.5 M_\odot \text{ yr}^{-1}$. Accounting for internal extinction would further increase the intrinsic $\text{H}\alpha$ and NUV fluxes. Star-formation, however, is most likely not the only heating and ionizing source in the cluster center.

The large turbulent velocities and the elevated $[\text{N II}]/\text{H}\alpha$ ratio of ~ 1.5 in the nucleus (Crawford & Fabian 1992) indicates that the interaction with the radio jets contributes strongly to the heating of the gas in the center. The $[\text{N II}]/\text{H}\alpha$ line ratios of 0.6 in the western filament are relatively high as well (Crawford & Fabian 1992), indicating the presence of an additional non-ionizing source of energy at larger radii (see e.g. Ferland et al. 2009).

Based on the data for M87, Werner et al. (2010) proposed that

the $\text{H}\alpha$ filaments in its core may be powered by shock induced mixing of cold gas with the surrounding ICM (see Begelman & Fabian 1990). By bringing the hot thermal particles into contact with the cool gas, mixing can supply the power and ionizing particles to explain the observed spectra. Hot ICM electrons that penetrate into the cold gas excite the molecular hydrogen and deposit heat. This scenario has been explored theoretically by Ferland et al. (2008, 2009), who studied heating by cosmic-rays, which affect the cooler ionized and neutral components in a similar way to hot ICM electrons. The fact that the soft X-ray emission traces the $\text{H}\alpha$ emitting gas suggests that this process could be responsible for part of the $\text{H}\alpha + [\text{N II}]$ line emission, part of the UV emission, and for the non-radiative cooling of the coldest X-ray gas in Sérsic 159-03.

The most similar known X-ray/ $\text{H}\alpha$ filament system is observed in Abell 1795. In that cluster the filament extends for 50 kpc . The cD galaxy at the head of this filament is moving with respect to the ICM and the emission line nebula may originate from a runaway cooling of the hot X-ray emitting gas in the wake of that motion (Fabian et al. 2001; Markevitch et al. 2001; McDonald & Veilleux 2009). The filamentary system in Sérsic 159-03, however, is most likely the result of AGN driven uplift and ram pressure stripping from the cD galaxy. The filament in Abell 1795 is composed of a pair of thin $w < 1 \text{ kpc}$ intertwined $\text{H}\alpha + [\text{N II}]$ filaments (McDonald & Veilleux 2009), spatially coincident with relatively cool X-ray emitting gas (Fabian et al. 2001), and with chains of FUV-bright young star clusters condensing from the cooling gas in the filament (Crawford et al. 2005; McDonald & Veilleux 2009). The northern end of the large $\text{H}\alpha$ filament in Sérsic 159-03 separates into two narrow, parallel structures. Given a better spatial resolution, we would most likely resolve the filament into more thin threads. As discussed by Fabian et al. (2008) for the emission line nebulae in the core of the Perseus Cluster, the thin thread-like filamentary structures are most likely stabilized by magnetic fields. These magnetic fields might be possible to detect using Faraday Rotation against the polarized jet emission (as has been done for the filaments in the Centaurus Cluster by Taylor et al. 2007).

4.3 The powerful radio mode AGN

The core of Sérsic 159-03 harbors a powerful radio mode AGN. Inflating the southern cavity required a $4pV$ work of about $7 \times 10^{58} \text{ ergs}$, indicating powerful jets. However, no optical or X-ray point source is presently seen at the position of the radio bright AGN. Using the ‘Black hole fundamental plane’ relation of Merloni et al. (2003), for a 10 mJy core flux at 4.75 GHz and for a black hole mass of $6 \times 10^8 M_\odot$ (determined from the K-band bulge luminosity by Rafferty et al. 2006), the expected X-ray core flux is $2.4 \times 10^{-13} \text{ erg s}^{-1} \text{ cm}^{-2}$. This value is two orders of magnitude higher than our conservative upper limit of $2.3 \times 10^{-15} \text{ erg s}^{-1} \text{ cm}^{-2}$. The observed scatter around the ‘Black hole fundamental plane’ is, however, large. The radio luminosities of some other well known brightest cluster galaxies (e.g. NGC 1275) also show similar offsets with respect to the expected relation.

The radio morphology is similar to 4C26.42 in Abell 1795 (Liu et al. 2009) and it is also reminiscent of PKS 1246-410 in the Centaurus Cluster (Taylor et al. 2007). The distortion of the jets, and the change in the axis from N-S to E-W, is most likely due to the strong interactions with the dense gas. The velocity dispersion of the NIR emission lines, which sharply increases in the nuclear region (Oonk et al. 2010) shows that the interaction of the jets with the cold gas is the strongest within the innermost 2 kpc region. The presence of cold, high density material in the cluster core is likely

to decelerate the jets, which might entrain thermal gas, slow down to subsonic velocities, and continue to rise buoyantly. Such deceleration due to strong interaction with dense gas on small scales has been seen using VLBA observations in Hydra A (Taylor 1996) and Abell 1795 (Liuzzo et al. 2009). While the 1.4 GHz and 617 MHz radio plasmas appear to be deflected by the dense ‘northern ridge of cooling plasma’ to the east, forming the ‘eastern elongated X-ray dark cavity’, the younger radio jet seen at 8.4 GHz is being deflected to the northwest where it is likely to continue to buoyantly rise along the short axis of the cluster. The 8.4 GHz southern jet is being deflected by the H α emitting gas to the southeast where it is partly filling the ‘southern X-ray cavity’.

Between 244 MHz and 1.4 GHz the integrated radio emission in the cluster core has a remarkably steep power-law spectrum $S_\nu \propto \nu^{-\alpha}$ with index $\alpha = 1.49$. At higher frequencies, however, the radio spectrum flattens to index $\alpha = 0.71$. At the 4.75 GHz ATCA radio map (Hogan et al. in prep.), the radio morphology is very similar to that at 8.4 GHz, indicating that the flatter part of the integrated radio emission originates in the ~ 10 kpc scale inner lobes (see the contours in the left panel of Fig. 3) where active jets are injecting relativistic particles. At the lower frequencies the radio emission is more extended, indicating an older population of electrons. The spectral index map produced from the 617 MHz and 1.4 GHz radio data (central panel of Fig. 3) shows that while in the central regions $\alpha \sim 1$, to the east, where the radio plasma seems to be filling the elongated cavity, the spectral index steepens to $\alpha > 2$. The spectral index also steepens in the northwest, where the plasma fills a region with a relative deficit in X-ray surface brightness. This radio plasma is most likely buoyant and exerting work on the surrounding medium.

The steep integrated spectrum of the radio source is similar to radio mini-halos found within the cooling radius of some clusters (e.g. Ferrari et al. 2008). The morphology of the extended radio emission, however, indicates that it is due to the plasma from the radio jets which have been decelerated, deflected and confined by the interaction with the dense gas. A steep radio spectral index has been found in other cooling core clusters (e.g., PKS 0745-191, A2029, A4059, A2597 Taylor et al. 1994; Pollack et al. 2005) and taken as an indicator of confinement.

Our thermodynamic maps show that the projected thermal pressure peaks in an approximate ring surrounding the AGN. The pressure in the ring is approximately 20 per cent higher than in the center. The high pressure region to the south of the AGN is hotter than the plasma both outside and inside this feature, strongly suggesting that it has been shock heated. The observed projected temperature jump of $\Delta T \sim 1.2$ suggests a shock with a Mach number of $M \sim 1.5$. The complex X-ray morphology with a cavity inside the shock front unfortunately prevents a more precise modeling of the shock. The relatively modest, factor of 1.5, temperature drop in the core of this cluster (Sun et al. 2009) also points towards a relatively strong AGN feedback activity. AGN induced shocks, which may be the most significant channel for heating of the ICM near to the AGN, have also been observed around M87 in the center of the Virgo Cluster and in Hydra A, (Forman et al. 2005; Million et al. 2010b; Nulsen et al. 2005; Simionescu et al. 2009b).

5 CONCLUSIONS

We performed a multi-wavelength study of the energetic interaction between the central active galactic nucleus (AGN), the intra-cluster

medium, and the optical emission line nebula in the galaxy cluster Sérsic 159-03. We conclude that:

- Powerful ‘radio mode’ AGN feedback and possible ram pressure cleared the central region of the cD galaxy ($r < 7.5$ kpc) of the cooling low entropy X-ray gas.
- This low entropy, high metallicity, relatively cool X-ray gas lies along the bright, 44 kpc long H α + [N II] filament extending from the centre of the cD galaxy to the north.
- As indicated by the observed dust lanes, molecular and ionized emission line nebulae, and the excess UV emission, part of this displaced gas, which is removed from the direct influence of the AGN, cools and forms stars.
- The pressure map shows evidence for an AGN induced weak shock at a radius of $r = 15$ kpc and the X-ray images reveal cavities indicating past powerful AGN activity with an energy of $\sim 7 \times 10^{58}$ ergs. At low frequencies, the radio source has an unusually steep spectrum with $\alpha = 1.5$ indicating aging and confinement by the ambient gas.

ACKNOWLEDGMENTS

We thank Alastair Edge and Michael Hogan for providing the reduced 4.75 GHz ATCA radio data and for helpful discussions. We thank Seth Bruch and Emily Wang for their help with the SOAR observations. Support for this work was provided by the National Aeronautics and Space Administration through Chandra/Einstein Postdoctoral Fellowship Award Number PF8-90056 and PF9-00070 issued by the Chandra X-ray Observatory Center, which is operated by the Smithsonian Astrophysical Observatory for and on behalf of the National Aeronautics and Space Administration under contract NAS8-03060, and by the Chandra grants GO0-11019X and GO0-11139X. This work was supported in part by the U.S. Department of Energy under contract number DE-AC02-76SF00515. The Very Large Array is part of the National Radio Astronomy Observatory. The National Radio Astronomy Observatory is a facility of the National Science Foundation operated under a cooperative agreement by Associated Universities, Inc. We thank the staff of the GMRT that made these observations possible. The SOAR Telescope is a joint project of Conselho Nacional de Pesquisas Científicas e Tecnológicas CNPq-Brazil, The University of North Carolina Chapel Hill, Michigan State University, and the National Optical Astronomy Observatory.

REFERENCES

- Baars J. W. M., Genzel R., Pauliny-Toth I. I. K., Witzel A., 1977, A&A, 61, 99
- Begelman M. C., Fabian A. C., 1990, MNRAS, 244, 26P
- Birzan L., McNamara B. R., Nulsen P. E. J., Carilli C. L., Wise M. W., 2008, ApJ, 686, 859
- Bland-Hawthorn J., Maloney P. R., 1999, ApJ, 510, L33
- Bock D., Large M. I., Sadler E. M., 1999, AJ, 117, 1578
- Buote D. A., 2000, ApJ, 539, 172
- Cardelli J. A., Clayton G. C., Mathis J. S., 1989, ApJ, 345, 245
- Crawford C. S., Fabian A. C., 1992, MNRAS, 259, 265
- Crawford C. S., Sanders J. S., Fabian A. C., 2005, MNRAS, 361, 17
- de Plaa J., Werner N., Bykov A. M., et al., 2006, A&A, 452, 397
- de Plaa J., Werner N., Simionescu A., Kaastra J. S., Grange Y. G., Vink J., 2010, A&A, 523, A81+

- Edwards L. O. V., Robert C., Mollá M., McGee S. L., 2009, *MNRAS*, 396, 1953
- Ehlert S., Allen S. W., von der Linden A., et al., 2010, *MNRAS*, 1802
- Fabian A. C., Johnstone R. M., Sanders J. S., et al., 2008, *Nature*, 454, 968
- Fabian A. C., Mushotzky R. F., Nulsen P. E. J., Peterson J. R., 2001, *MNRAS*, 321, L20
- Fabian A. C., Sanders J. S., Allen S. W., et al., 2003, *MNRAS*, 344, L43
- Ferland G. J., Fabian A. C., Hatch N. A., et al., 2008, *MNRAS*, 386, L72
- Ferland G. J., Fabian A. C., Hatch N. A., et al., 2009, *MNRAS*, 392, 1475
- Ferrari C., Govoni F., Schindler S., Bykov A. M., Rephaeli Y., 2008, *SSR*, 134, 93
- Forman W., Nulsen P., Heinz S., et al., 2005, *ApJ*, 635, 894
- Greisen E. W., 2003, *Information Handling in Astronomy - Historical Vistas*, 285, 109
- Grevesse N., Sauval A. J., 1998, *Space Science Reviews*, 85, 161
- Hicks A. K., Mushotzky R., 2005, *ApJ*, 635, L9
- Kaastra J. S., Ferrigno C., Tamura T., Paerels F. B. S., Peterson J. R., Mittaz J. P. D., 2001, *A&A*, 365, L99
- Kaastra J. S., Mewe R., Nieuwenhuijzen H., 1996, in *UV and X-ray Spectroscopy of Astrophysical and Laboratory Plasmas* p.411, K. Yamashita and T. Watanabe. Tokyo : Universal Academy Press
- Kaastra J. S., Tamura T., Peterson J. R., et al., 2004, *A&A*, 413, 415
- Kalberla P. M. W., Burton W. B., Hartmann D., et al., 2005, *A&A*, 440, 775
- Kennicutt Jr. R. C., 1998, *ApJ*, 498, 541
- Large M. I., Mills B. Y., Little A. G., Crawford D. F., Sutton J. M., 1981, *MNRAS*, 194, 693
- Liuzzo E., Taylor G. B., Giovannini G., Giroletti M., 2009, *A&A*, 501, 933
- Magorrian J., Tremaine S., Richstone D., et al., 1998, *AJ*, 115, 2285
- Maia M. A. G., da Costa L. N., Willmer C., Pellegrini P. S., Rite C., 1987, *AJ*, 93, 546
- Markevitch M., Vikhlinin A., Mazzotta P., 2001, *ApJ*, 562, L153
- Mauch T., Murphy T., Buttery H. J., et al., 2003, *MNRAS*, 342, 1117
- McDonald M., Veilleux S., 2009, *ApJ*, 703, L172
- McDonald M., Veilleux S., Rupke D. S. N., Mushotzky R., 2010, *ApJ*, 721, 1262
- McNamara B. R., Nulsen P. E. J., 2007, *ARA&A*, 45, 117
- Merloni A., Heinz S., di Matteo T., 2003, *MNRAS*, 345, 1057
- Million E. T., Allen S. W., Werner N., Taylor G. B., 2010a, *MNRAS*, 405, 1624
- Million E. T., Werner N., Simionescu A., et al., 2010b, *MNRAS*
- Nulsen P. E. J., McNamara B. R., Wise M. W., David L. P., 2005, *ApJ*, 628, 629
- Oonk J. B. R., Jaffe W., Bremer M. N., van Weeren R. J., 2010, *MNRAS*, 405, 898
- Pollack L. K., Taylor G. B., Allen S. W., 2005, *MNRAS*, 359, 1229
- Quillen A. C., Zufelt N., Park J., et al., 2008, *ApJS*, 176, 39
- Rafferty D. A., McNamara B. R., Nulsen P. E. J., Wise M. W., 2006, *ApJ*, 652, 216
- Randall S. W., Forman W. R., Giacintucci S., et al., 2011, *ApJ*, 726, 86
- Sanders J. S., 2006, *MNRAS*, 371, 829
- Sanders J. S., Fabian A. C., Frank K. A., Peterson J. R., Russell H. R., 2010, *MNRAS*, 402, 127
- Sanders J. S., Fabian A. C., Taylor G. B., 2009, *MNRAS*, 396, 1449
- Sharma P., Parrish I. J., Quataert E., 2010, *ApJ*, 720, 652
- Shepherd M. C., Pearson T. J., Taylor G. B., 1995, in *Bulletin of the American Astronomical Society*, edited by B. J. Butler & D. O. Muhleman, vol. 27 of *Bulletin of the American Astronomical Society*, 903
- Simionescu A., Roediger E., Nulsen P. E. J., et al., 2009a, *A&A*, 495, 721
- Simionescu A., Werner N., Böhringer H., et al., 2009b, *A&A*, 493, 409
- Sirothia S. K., 2009, *MNRAS*, 398, 853
- Sun M., Donahue M., Voit G. M., 2007, *ApJ*, 671, 190
- Sun M., Voit G. M., Donahue M., Jones C., Forman W., Vikhlinin A., 2009, *ApJ*, 693, 1142
- Taylor G. B., 1996, *ApJ*, 470, 394
- Taylor G. B., Barton E. J., Ge J., 1994, *AJ*, 107, 1942
- Taylor G. B., Fabian A. C., Gentile G., Allen S. W., Crawford C., Sanders J. S., 2007, *MNRAS*, 382, 67
- Werner N., Simionescu A., Million E. T., et al., 2010, *MNRAS*, 407, 2063